Iranian Journal of Science and Technology, Transactions of Electrical Engineering (2023) 47:1447–1457
https://doi.org/10.1007/s40998-023-00643-4

RESEARCH PAPER

Investigating the Tradeoff Between the MMF Distortion and End Turn Length of a 2-Pole Line Start SynRM Performance

Didem Tekgun[1] · Muhammed M. Cosdu[1] · Burak Tekgun[1] · Irfan Alan[1]

Received: 15 December 2022 / Accepted: 29 June 2023 / Published online: 19 July 2023

Abstract
Conventional 2-pole AC machine windings have long end windings and generate harmonics, which increase losses and reduce torque density. This study investigates the performance tradeoff between the level of distortion (THD) in winding magneto-motive force (MMF) and end turn length on a 2-pole line start Synchronous Reluctance Machine (LS-SynRM) machine. A two-stage approach is used, winding and geometry optimization. Various multilayer winding configurations having unevenly distributed number of turns are investigated. First, the percentage of the turns in a coil group is optimized for minimum harmonics and end turn length for all structures. Second, geometric optimization is performed on selected winding configurations. Sixteen different configurations are optimized, and Pareto optimal solutions are obtained. Later, these solutions are graded with a new score-based assessment method to quantify the quality of the results. It is concluded that the designs having lower THD in winding MMF perform better than the designs with shorter end turns in terms of efficiency and torque density.

Keywords Winding MMF harmonics · Multi-objective optimization · Differential evolution · End winding optimization · Reluctance machine

1 Introduction

Recently, due to the ongoing increase in the global population, the demand of reducing energy consumption is a common goal all around the world. Since global warming is a big issue to control, sustainable and green technologies are needed to be consumed consciously. Energy consumption of electrical machines and drive systems corresponds to 70% of electrical energy production worldwide (De et al. 2014). Hence, there is a growing demand for more efficient, compact, and robust motor designs especially running in the low and mid-power range (Stojceska et al. 2022). Motors that are used for the purposes of industrial, domestic, and irrigation mostly are working in this power range. A major part of the energy is consumed by the water pump systems used for irrigation purposes (De et al. 2014).

For water pump applications, Induction Machine (IM) is mostly the first choice due to its robust and reliable structure, line start, and low-cost features. However, IM used in submersible water pumps has a quite low efficiency. Although Permanent Magnet Synchronous Machines (PMSM) with superior efficiency are available in the market, their high cost and environmental concerns like rare earth material dependency make this machine less favorable. Moreover, the problems like degradation of the magnet field over time and permanent demagnetization require magnet renewal or re-magnetizing, making the PMSM less favorable.

Being an alternative to the IM, Synchronous Reluctance Machine (SynRM) reaches high-efficiency levels. Still, SynRM requires a drive system like the PMSM. Thus, Line Start SynRM (LS-SynRM) comes forward as a good alternative to the IMs as it can both start with line voltage and does not have any rare earth permanent magnet. Thanks to the squirrel cage existing in the rotor, LS-SynRM can start like an IM. When it gets close to the synchronous speed, it synchronizes and generates a torque due to its rotor's salient structure. When it is operating at

✉ Burak Tekgun
burak.tekgun@agu.edu.tr

[1] Department of Electrical and Electronics Engineering, Abdullah Gul University, Kayseri 38080, Turkey

the synchronous speed, the squirrel cage does not carry any current; hence, it does not cause any rotor losses. Also, the torque and power density of SynRM is higher than IM (Mingardi and Bianchi 2017). Consequently, LS-SynRM reliable, efficient, and low-cost alternative to the PMSM and IM. Nonetheless, SynRM has two major drawbacks: excessive torque ripple and poor power factor (Bianchi et al. 2009; Lipo 1991; Vagati et al. 1998; Kim et al. 2020). Several number of multi-barrier rotor optimization studies for SynRMs exist in the literature which are aiming torque ripple reduction (Vagati et al. 1998) and power factor improvement (Kim et al. 2020). Additionally, various optimization methods of SynRMs are investigated in Cupertino et al. (2014) and Sato et al. (2015). In the aforementioned optimization studies, the same winding structure as in standard IMs is used in the stator.

Designing a machine with proper winding configuration is one of the major challenges since the winding structure has an important effect on the machine performance. It becomes more challenging for 2-pole AC machines compared to the higher pole count machines. Winding Magneto-Motive Force (MMF) harmonics induce increased copper and core losses along with mechanical vibration, and acoustic noise (Kurihara et al. 1994; Dajaku et al. 2014, 2019). A proper winding configuration with low harmonic content MMF winding results in significantly improved motor performance (Kocabas 2009; Gundogdu and Komurgoz 2019; EL-Refaie AM 2010). Since the space harmonics are inherently caused by the harmonic distortion of a specific winding distribution, having more sinusoidal winding MMF provides less torque ripple and a higher power factor. In the literature, reducing the MMF harmonics is also selected as the optimization objective for the two types of windings; one is distributed (Kocabas 2009), and the other one is fractional-slot concentrated windings (FSCWs) (EL-Refaie AM 2010; Dajaku and Gerling 2012). Some FSCW topologies are introduced to reduce the dominant harmonics, including multilayer structures (Cistelecan et al. 2010), dual multiphase winding configurations (Abdel-Khalik et al. 2015), and unequal turns per coil winding configurations (Cistelecan et al. 2010). Moreover, FSCW design optimizations are integrated the some of the winding studies to maximize the fundamental of MMF and minimize the winding MMF total harmonic distortion (THD) (Bekka et al. 2016).

Recently, a few studies have reported related to SynRM designs with concentrated windings (Spargo et al. 2013). Major advantages of concentrated windings are non-overlapping, high slot fill factor, and short end-turn length. On the other hand, the winding MMF harmonic contents are increased significantly in concentrated winding structures. These harmonics end up with a reduced power factor, higher ripple on torque, and increased copper losses; hence, the efficiency is reduced significantly (Spargo et al. 2013; Gamba et al. 2015). Several 3-phase winding structures are proposed in the literature to reduce space harmonics (Vagati et al. 1998; Cistelecan et al. 2010). Although the 5th order harmonic helps improve the torque production, additional 7th, 17th, and 19th order harmonics degrade the torque production. Accordingly, the number of poles and stator slots are needed to be increased (Cistelecan et al. 2010). However, increasing the number of poles results in a higher fundamental frequency and increased core loss, while the power factor decreases (Kabir and Husain 2016). Another type of winding configuration with multiple layers (ML) is proposed in Kabir and Husain (2018) for SynRM. The proposed ML winding configuration reduces torque ripple while improving the power factor. Shorter end winding lengths and low MMF THD is obtained using this winding scheme. However, there is only the triple-layer winding structure where all the slots contain all three phase windings is investigated, while the double-layer configurations, which could be favorable, are not considered.

The paper explores the tradeoff between the winding MMF THD and the length of the end turns with regard to the synchronous performance of a 2-pole, 4-kW, LS-SynRM. The study considers different multi-layer winding structures, including basic single-layer winding, various double-layer windings, and three-layer windings, all designed for a 24-slot stator. These windings feature an uneven number of turns in each coil. The optimization study is conducted in two steps: first, the winding is optimized, and second, the geometry is optimized. The study uses the Multi-Objective Differential Evolution (MODE) algorithm to optimize both the winding and geometry of the LS-SynRM. In the first step, the winding MMF THD and end winding lengths are optimized for each of the winding configurations. The end winding length is evaluated using an indicator called the end winding score (EWS). The winding optimization results provide a Pareto front solution set showing the tradeoff between the THD and the EWS for each winding configuration, which features an uneven distribution of different coils. A total of sixteen designs are considered for the geometric optimization. Here, the optimization objectives are selected as minimizing the losses and the mass; hence, maximizing the machine efficiency and the torque density. Following the geometric optimization, sixteen Pareto optimal solution sets are obtained for each winding configuration with different coil turn ratios. These results provide insights into how winding MMF THD and end winding length affect the motor's performance in terms of efficiency and mass. However, quantifying the quality of each design's Pareto frontier solution set can be a tedious process. To address this issue, a score-based quality assessment method is proposed. The first score is the average of overall efficiency

per mass, and the second is the average of inverse torque ripple for each Pareto frontier.

This paper is organized as follows: The proposed winding configurations are introduced in Sect. 2 where the winding functions and harmonic analyzes are performed. The design optimization process is explained in Sect. 3, results and discussions are provided in Sect. 4. Section 5 gives the details of the score based quality assessment method and the paper is concluded in Sect. 6.

2 Proposed ML Winding Configurations

In this section, various ML winding configurations and their analysis in terms of winding MMF harmonics are presented.

2.1 ML Winding Concepts

In 2-pole AC machines, the standard winding structure has a long throw that causes a high end winding resistance and has a high harmonic content on the winding MMF. It is possible to improve the machine efficiency by reducing the harmonic contents of the stator field, but this may lead to an increased end winding resistance and cancel out all the benefits gained through THD improvement. This is a tradeoff and needs to be analyzed further. In order to generate an MMF that has low harmonic distortion, while shortening the end winding conductor length, the uneven number of turns method is introduced in Cistelecan et al. (2010); Tessarolo et al. 2016). However, for a 24 slot, single-layer winding configuration, there are only 2 coils in a pole that does not have enough freedom to adjust the number of turns and slot locations for each coil to improve the THD and the end winding resistance.

The double-layer and triple-layer configurations are recognized as practical options for coil distribution and turn count variation, which can effectively mitigate the harmonic content of the winding MMF and minimize the resistances of the end winding (Tekgun et al. 2021). In this study, we consider a 24-slot stator and investigate the conventional even number of turn single-layer, four distinct double-layer, and one triple-layer configuration that employs windings with uneven numbers of turns. The single pole rectilinear winding layouts of the considered winding configurations are presented in Fig. 1.

2.2 Winding Function Analysis

The Stator MMF aims to create a rotating magnetic field with a sinusoidal distribution in the air gap. To achieve a sinusoidal flux density, a sinusoidal MMF is required (Lipo 2017). However, the rotor saliency plays a significant role in influencing the airgap flux density, even if the stator MMF is pure sinewave, airgap flux density distribution varies with salient and non-salient pole machines, which has a significant effect on the machine performance (Barcaro and Bianchi 2010). In salient pole machines, the goal is to minimize the distortion of the airgap flux density, which begins with ensuring the stator MMF is as sinusoidal as possible. In (Kabir and Husain 2018), the winding optimization of a triple layer winding SynRM is performed to determine the optimal coil turn percentages that yield the lowest MMF THD, and shorter end turn length.

AC winding factor, k_{wv}, is presented as the multiplication of the distribution factor, k_{dv}, and the pitch factor, k_{pv}, at the v^{th} harmonic. Fluxes of the distributed coils and the same pitched coils intersect each other indirectly with a phase shift described in Eq. (1) for a single-phase. Here, α is the phase shift angle ($\alpha = \pi/mq$, where m is machine phase number), q is the number of slots, and τ_p is the pole pitch. Equation (2) shows the number of turns at each phase which is expressed as N_{ph}. Winding factor k_{wv} in Eq. (3) expresses the MMF harmonics where the stator MMF is expressed as in Eq. (4). When all coil sets MMF are in phase, k_{dv} will be counted as 1 for each harmonic. Hence, the peak harmonics produced by all three phases are expressed in Eq. (5) and (6).

Here, v is the harmonic order ($1 \pm 6c$), where c is an integer, n is the number of coils, N_n is the number of turns for the n^{th} coil group, q_n is the number of coils in a coil group per pole pair, p represents the number of pole pairs and, i_s is the phase current (Pyrhönen et al. 2008).

$$k_{dv} = \frac{\sin(v\frac{q.\alpha}{2})}{q.\sin(v\frac{\alpha}{2})} \tag{1}$$

$$N_{ph} = \sum_n N_n.q_n \tag{2}$$

$$k_{pv} = \frac{1}{N_{ph}}\sum_n N_n.q_n.\sin(v.\frac{2n-1}{\tau_p}.\frac{\pi}{2}) \tag{3}$$

$$k_{wv} = k_{pv}.k_{dv} \tag{4}$$

$$F_{st}^v = \frac{3}{\pi.v}.\frac{N_n}{p}.k_{wv}.i_s \tag{5}$$

$$F_{st}^v = \frac{3}{\pi.v}.\frac{N_{ph}}{p}.k_{pv}.i_s \tag{6}$$

2.3 Harmonic Analysis

As mentioned before, achieving a low THD winding MMF with single-layer winding is a quite challenging task as there are only two coils in a 24 slot 2-pole configuration. In Fig. 2a, the winding MMF distribution and its Fourier transform along with the related THD value are provided

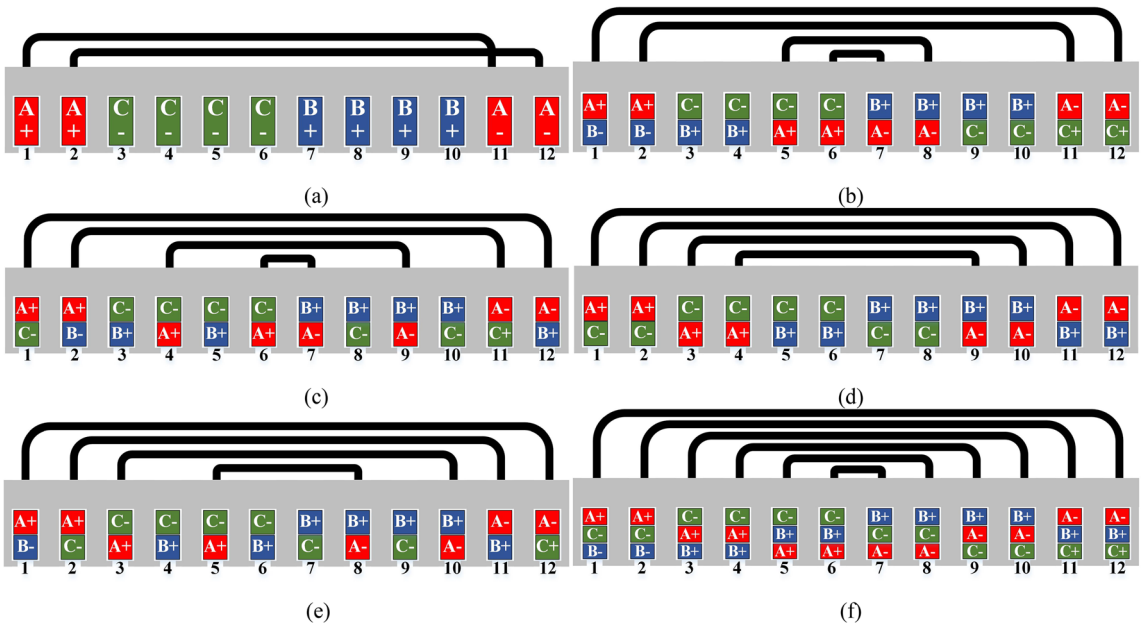

Fig. 1 Single pole rectilinear winding layout for **a** single-layer, **b** first, **c** second, **d** third, **e** fourth version of the double-layer, and **f** triple-layer windings

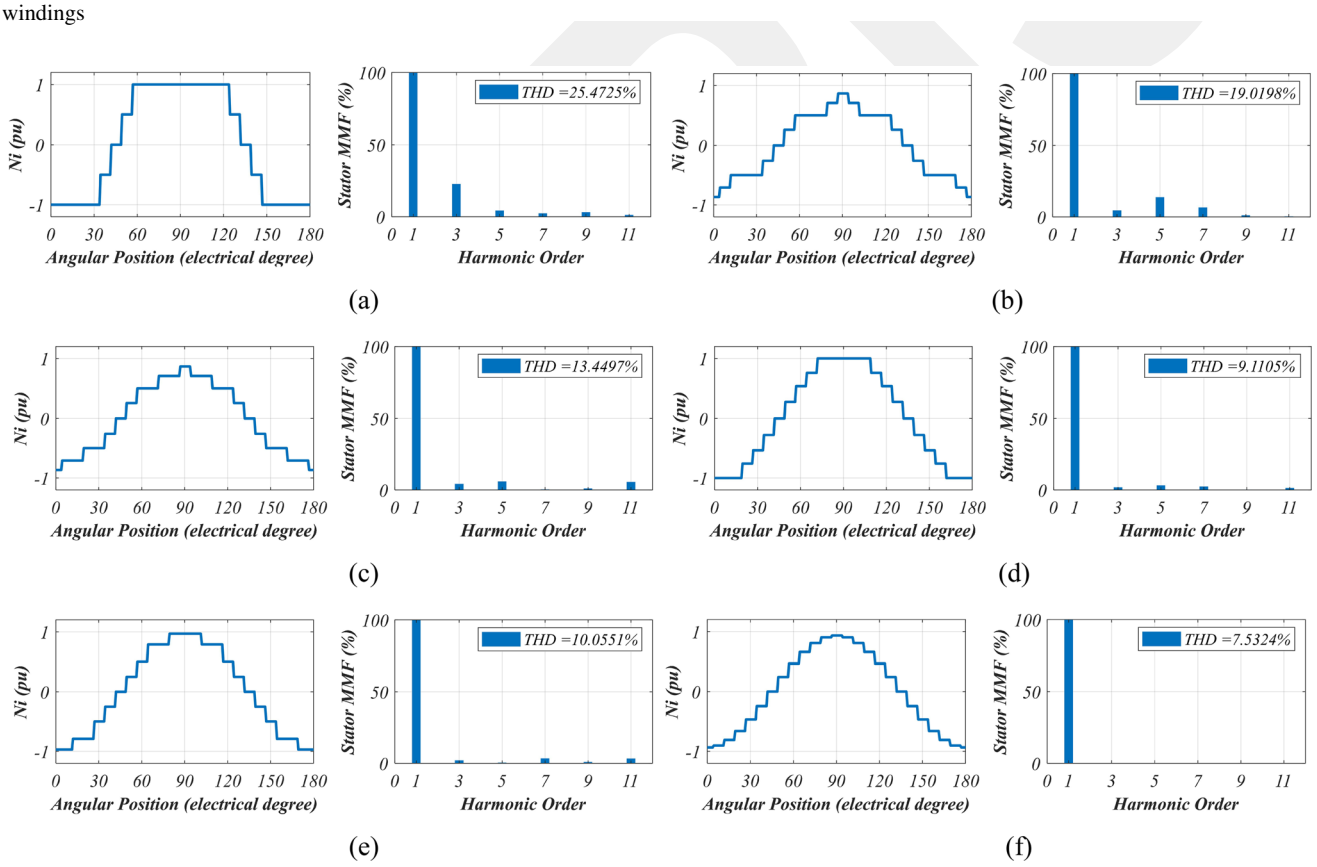

Fig. 2 MMF distributions and the FFT of the **a** single-layer, **b** first, **c** second, **d** third, **e** fourth version of the double-layer, and **f** triple-layer windings

for a single layer winding configuration and an even number of turns. As the layer count increase, there is more freedom for adjusting the coil positions and the number of turns to get a low THD. For the same slot-pole configuration, there are 4 coils in a pole that reaches the peak MMF value in four steps. Taking the uneven number of

turns into account, the MMF distribution can even have a less harmonic content. However, it should be kept in mind that as the number of winding layers increases, so does the manufacturing complexity and cost. In Fig. 2b–e, different double-layer winding configurations' MMF distributions, Fourier transforms, and THDs are provided. It can be seen that the THD values are lower compared with the single-layer configuration. In Fig. 2f, the results of the triple-layer configuration are presented where the best THD value is achieved. However, having a low harmonic content stator field may not be the optimal solution as having multiple layers may lead to longer end winding conductor length and higher phase resistance. This could result in lower efficiency. It is clear that there is a tradeoff between the MMF THD and end winding resistance. There should be an optimization process to analyze this phenomenon.

3 Design Optimization

In this section, the design optimization procedure is explained in stages. The workflow of the optimization process is illustrated in Fig. 3. In the first stage, a series of winding optimization studies are carried out with the MODE algorithm in MATLAB. In this stage, each coil group's number of turn ratios with respect to the total number of turns per pole per phase are determined subject to the minimum THD of the winding MMF and minimum EWS objectives, which are determined through analytical computations. As a result of this step, six Pareto front sets are obtained for six winding configurations. Subsequently, three distinct results from these Pareto frontier sets are selected: the one with the minimum THD, one with the minimum EWS and less than 20% THD, and the one in between. The reason selecting these three results is to distinguish the influence of the winding MMF harmonic content and the end turn length on the efficiency, torque density, and torque ripple of an LS-SynRM. During the second optimization stage, the rotor geometry, number of turns, stack length, current and current density are optimized for all candidate winding configurations, while the 2D stator geometry is kept the same to ensure a fair comparison. The optimization objectives in the second stage are to minimize the mass and loss and, hence, to maximize the torque density and efficiency of the motor. This procedure is explained in detail in Sects. 3.1 and 3.2.

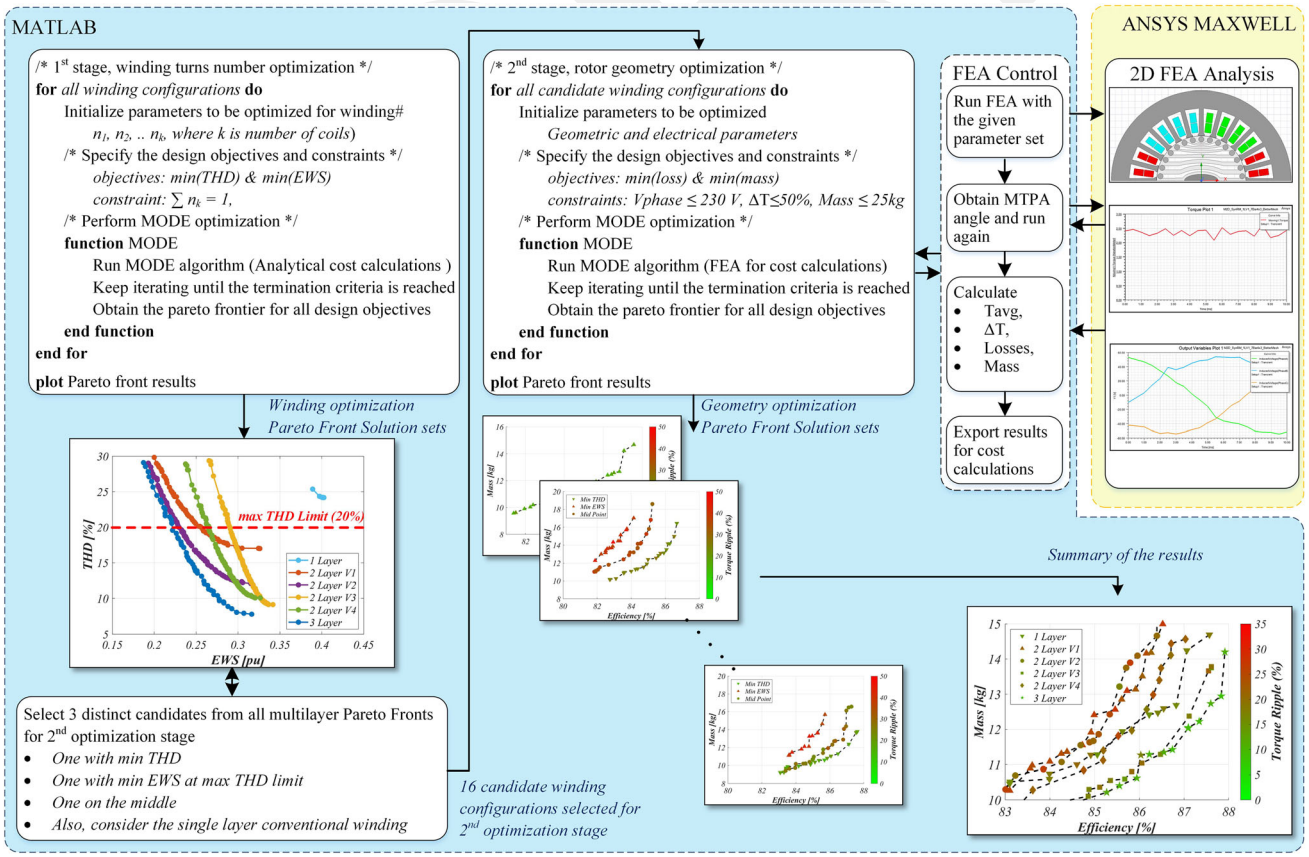

Fig. 3 Flow diagram of the proposed design optimization method

3.1 Winding Optimization

A 2-pole structure of LS-SynRM is required for a pump motor application as it can operate at 3000 rpm at 50 Hz line frequency and voltage. However, the length of the end turns is long and the winding MMF harmonic content is high with the single-layer conventional winding, especially in 2-pole motor structure.

In this study, various multiple level winding configurations are analyzed and compared to reduce the winding MMF harmonic content and decrease the total end winding length. An optimization algorithm is created to determine the percentages of the number of turns in each coil in a coil group. Optimization parameters are chosen to have individual weights of less than one but sum up to the one in total for each coil. Hence, the total number of turns for a coil group can be used as an optimization parameter and each individual coil turns can be calculated using the optimized ratios in the winding optimization stage.

There are two objectives for the winding optimization stage namely THD and EWS, which are formulated as (Pyrhönen et al. 2008):

$$THD = \frac{\sqrt{\left(F_{st}{}^{5}\right)^2 + \left(F_{st}{}^{7}\right)^2 + \left(F_{st}{}^{11}\right)^2 + \left(F_{st}{}^{13}\right)^2 + \ldots}}{F_{st}{}^{1}} = \frac{\sqrt{\left(\sum_{m=1}^{6}\right).\left(F_{st}{}^{6m\pm1}\right)^2}}{F_{st}{}^{1}} \tag{7}$$

$$EWS = \sum_{n}\left(\frac{l_{arc,n}}{l_{WP}} + l_{end,ext,n}\right)k_n \tag{8}$$

where F_{st} is the winding MMF, $l_{arc,\mathrm{n}}$ is the end winding arc length of the n^{th} coil, l_{WP} is the length of the circle passing the stator slot mid-points, $l_{end,\mathrm{ext,n}}$ is the end extension of each coil, and k_n is the proportional of the n^{th} coil number turn to the total number of turn. Figure 4 illustrates the phase-A end winding distribution in a double layer winding configuration shown in single pole rectilinear form.

3.2 Geometry Optimization

Merely determining the coil turn number ratios for the given winding configurations in the first optimization stage is insufficient to evaluate the performance of a machine. Hence, in the second optimization stage, the motors with the winding configurations that have been selected for their coil ratios in the first optimization stage are optimized using the MODE optimization algorithm. The optimization algorithm optimizes various parameters such as the rotor geometric parameters, total number of turns in one pole, stator stack length, phase current, and current density in one slot. In order to reduce the computational burden, only three candidate winding designs for each multilayer winding configuration are selected to perform the geometric optimization. The three candidate winding designs represent the minimum possible THD, the minimum possible EWS, and a mid-point between these two points. Hence, one conventional single layer, twelve double-layer with four different winding configurations and three different winding ratios, and three triple-layer winding configurations with three different winding ratios, a total of 16 candidate designs are taken to the geometric optimization stage. The FEA is performed in Ansys Maxwell 2D platform. Initially, there are many geometric parameters that complicate the optimization process and reduce the computation efficiency. Thus, the geometric parameters are defined as varying with ratio parameters which resulted in seven geometric ratio parameters. The geometric parameters are presented in Fig. 5 and the parameters used in the optimization are presented in Table 1.

In addition to the geometric parameters, phase current and current density are included in the optimization with their maximum boundaries. A 24-slot stator configuration and its shape are kept the same for all designs for a fair and direct comparison between each winding configuration and conventional structure. Here, the stator yoke radius, r_{MO}, is 68 mm, the inner radius of the stator, r_{RO}, is 34 mm, the stator tooth width, l_{TW}, is 3.2 mm, and the slot depth, l_{SD}, is 20.5 mm. The airgap, g, and rotor outer clearance, l_{OC} are

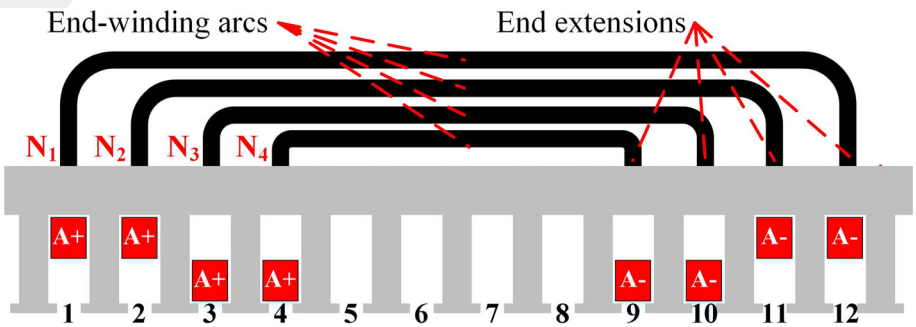

Fig. 4 Phase-A end winding illustration of a double layer winding configuration shown in single pole rectilinear form

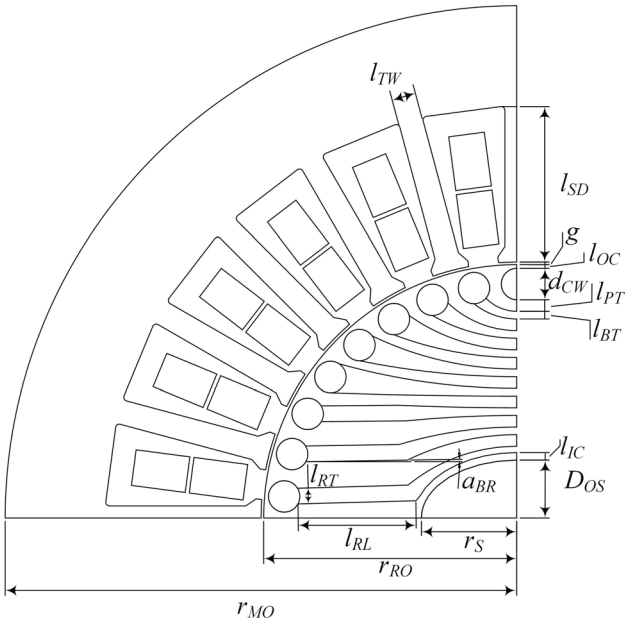

Fig. 5 The geometric parameters of the LS-SynRM

fixed at 0.35 mm and 0.5 mm, respectively, based on the manufacturing tolerances.

Here, the machine shaft is narrowed in the q-axis direction to widen the flux path and; therefore, to improve the saliency ratio. In (Tekgun and Alan 2022), the authors have carried out a series of structural, harmonic, and electromechanical analyzes to determine the limits of the reduced shaft size along with the analysis of the effect of the synchronization capability. Further explanations and calculations can be found in Tekgun and Alan (2022).

The optimization consists of two dependent parameters namely the stack length, l_{stack}, and the total number of turns of the coil groups, N_t. The machine is expected to provide 4 kW power at 3000 r/min speed, so the output torque should be 12.75 Nm and this torque value is directly proportional to the stack length. Thus, during the FEA analysis, the stack length is kept constant at 25 mm. Later this value is scaled based on the developed torque with a 25 mm stack length. The effect of the stack length is not only on the produced torque but also, on the induced back EMF voltage; hence, it is scaled with the stack length, too.

The other dependent parameter is the total number of turns of a coil group. To calculate this number, the RMS motor current, I_{rms}, current density, J, and available slot area, A_{slot}, are used for each variation. The fill factor, k_{fill}, is selected as 0.35 as a good industrial practice.

$$N_t = \frac{J \times I_{rms}}{A_{slot} \times k_{fill}} \tag{9}$$

The MODE algorithm progresses based on several objectives and constraints. This study considers maximizing the machine efficiency and minimizing the motor mass as the objectives. Machine efficiency was determined by calculating the machine losses in FEA software as given in the following expression where P_{out} is being the output power.

$$\eta = \frac{P_{out}}{P_{out} + Total\,Losses} \tag{10}$$

As the machine is intended to work with the line voltage, the terminal voltage should be within a 5% band. Therefore, the voltage of the machine along with the torque ripple are selected as constraints. In addition to these, motor mass is included in the constraint list to select reasonable results from the solution set for manufacturing. The expressions of the constraints are provided in Table 2.

Here, $e\angle\emptyset°$ is referred to as the back emf voltage, $I\angle\delta°$ is the phase current, r_s is the phase resistance, X_L is the leakage inductance reactance, ΔT is peak to peak variation of the torque waveform, and T_{avg} is the average torque,

Table 1 Optimization parameters

Parameter	Definition	Boundaries
a_{BR} (degree)	Bar rectangular section tilt angle	0–10
l_D (mm)	Shaft Radius (r_S) − *Elliptic Shaft Radius* (r_{ES})	0–5
l_{IC} (mm)	The distance between the shaft and the first flux barrier	1–5
k_B	$\frac{\text{Barrier Thickness } (l_{BT})}{\text{Plate Thickness } (l_{PT})}$	0.16–0.6
k_C	$\frac{\text{Rotor Conductor Diameter } (d_{CW})}{\text{Maximum Rotor Conductor Diameter}}$	0.67–0.85
k_R	$\frac{\text{Rectangular Barrier Length } (l_{RL})}{\text{Maximum Possible Length}}$	0.5–0.9
k_{REC}	$\frac{\text{Rectangular Barrier Thickness } (l_{RT})}{\text{Cage Cylinder Diameter } (d_{CW})}$	0.36–0.76
J (A/mm^2)	Current density	4–13
I_{peak} (A)	Motor current amplitude	5–15

Table 2 Constraints

Constraints	Expression	Limits
Peak phase voltage (V)	$\max(e\angle\emptyset^{\circ} + I\angle\delta^{\circ} \times (r_s + \mathrm{j}X_L))$	310–340
Torque ripple (%)	$\frac{\Delta T}{T_{avg}} \times 100$	0–50
Motor mass (kg)	$(A_{Stator} + A_{Rotor}) \times L_{stack} + M_{Copper}$	0–25

A_{stator} and A_{rotor} are the stator and rotor areas, L_{stack} is the stack length, and M_{Copper} is the copper mass.

4 Results

In the first stage of this study, the coil turn number ratios for different winding configurations are optimized with the MODE algorithm. The objectives are calculated analytically. Figure 6 displays the Pareto front of the different winding structures. Based on the findings, a trade-off between THD and EWS is noticeable. Decreasing one parameter will result in an increase in the other.

For the second stage optimization, a total of sixteen candidate winding configurations were chosen, with one being the conventional single layer configuration and the remaining fifteen consisting of three different turn number ratios from each of the five multilayer winding configurations. These three distinct turn number ratios are selected as: the one with the minimum THD, one with the minimum EWS and less than 20% THD, and the one in between. The computations were carried out using Ansys Maxwell FEA software, while the MODE algorithm was implemented in MATLAB and established communication with the FEA software via ActiveX scripts.

The second stage optimization is performed with the objective of minimizing the motor mass and loss. The results of this optimization are summarized in Fig. 7, with each part of the figure presenting the Pareto fronts of a specific winding configuration. Figure 7a displays the Pareto front of the machine with a single-layer winding configuration, which has only one Pareto front since the geometry optimization was performed for an even number of turns in each coil. Figures 7b–e illustrate the optimization results of machines with the first, second, third, and fourth versions of double-layer windings, respectively. Finally, Fig. 7f shows the Pareto front results of the machine with the triple-layer windings. For the multilayer windings, three optimization results are presented since, for all multilayer winding configurations, three distinct coil turn number ratios are used.

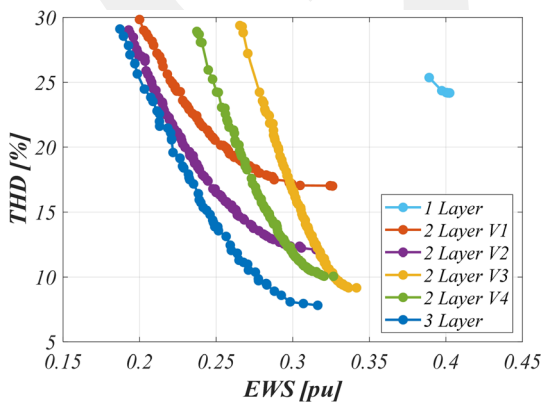

Fig. 6 THD-EWS result in various winding configurations

The results indicate that the third version of the double-layer winding and triple-layer winding outperformed the other configurations across the entire distribution. In certain cases, the efficiency improvement was as high as 2 points. Moreover, the triple-layer and third version of double-layer windings showed a significant improvement in torque ripple, which will enhance the reliability and life cycle of the machine.

Efficiency and torque ripple generally improve as the winding MMF harmonic content decreases. While reducing the end winding length can lead to a reduction in copper loss, an increase in winding MMF THD level can have a more significant impact on torque production. This trend is observed across all configurations. Figure 8a presents all the Pareto optimal solution sets with minimum winding MMF THD for summary and comparison purposes. Based on these results, it can be concluded that configurations that prioritize reducing winding MMF THD yield better performance compared to those with shorter end winding lengths.

Considering the SynRM is a reluctance machine that is sensitive to magnetic field distortion significantly, the findings align with the expectations. The configurations that have lower winding MMF THD have a better Pareto frontier solution set than the others. As a result, the triple-layer, and the double-layer third version configurations have better results than the other configurations in terms of efficiency, torque ripple, and motor mass.

5 Pareto Front Quality Assessment Method

After obtaining the Pareto frontier solutions for all the winding structures are considered, a quality assessment method is used to quantify the quality of the Pareto front results. Since the optimization objective can be

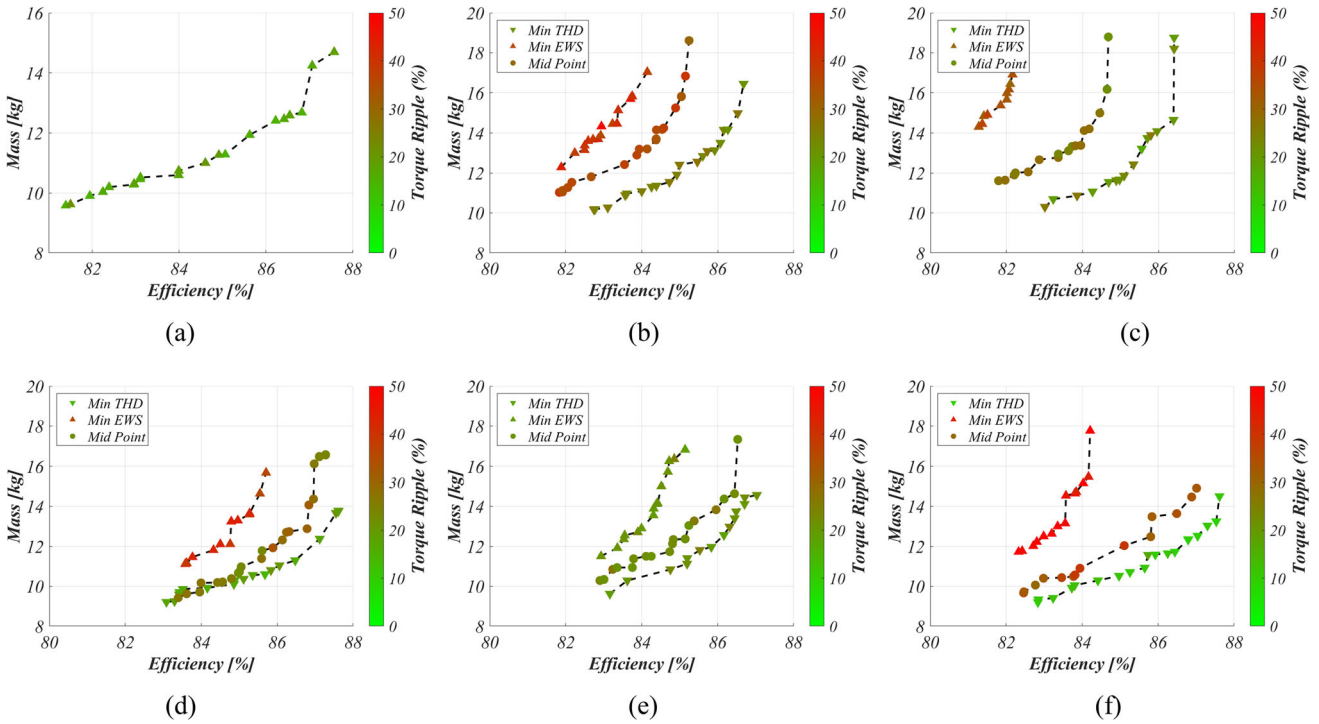

Fig. 7 Second stage optimization results of the **a** single-layer, **b** first, **c** second, **d** third, **e** fourth version of the double-layer, and **f** triple-layer windings

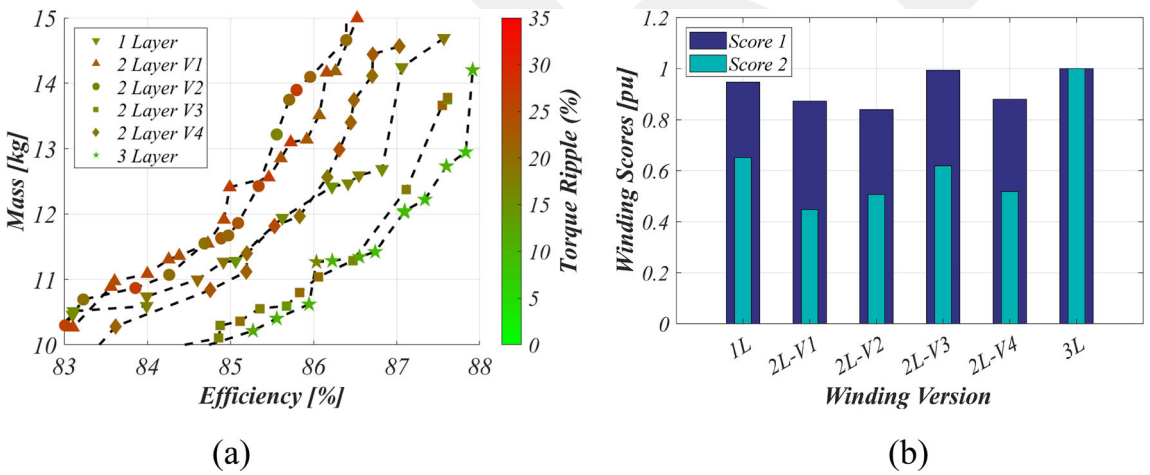

Fig. 8 **a** Comparison of Pareto front solutions and the **b** score-based quality comparison

summarized as maximizing the efficiency while minimizing the mass and the torque ripple, assessment scores are proposed as follows:

$$S_1 = \frac{1}{n}\sum_{k=1}^{n}\left(\frac{Efficiency_k}{Mass_k}\right) \tag{11}$$

$$S_2 = \frac{1}{n}\sum_{k=1}^{n}\left(\frac{1}{\Delta T_k}\right) \tag{12}$$

The primary score, S_1, is being the average value of the efficiency over the mass of a specific winding configuration Pareto frontier solutions. The secondary score, S_2, is the average value of the inverse of the torque ripple, ΔT^{-1}, where k is the number of the candidate designs in a Pareto frontier solution set for a specific winding configuration. Due to the way that these assessment scores are defined, a higher score means a better winding configuration. The reason the scores are named as primary and secondary is to highlight the importance of the score, the efficiency over the mass ratio is more important than the inverse of the torque ripple for the specific application. In order to distinguish the variation of the scores over the considered

winding configurations and compare them easily, the calculated scores are normalized and plotted as shown in Fig. 8b.

In terms of the primary score, the triple-layer winding performed the best followed by the double-layer version 3, and single-layer winding configurations. Similarly, the best-performed configuration is the triple-layer configuration in terms of the secondary score which is followed by the single-layer and double-layer version 3 ones. At this point, prioritizing the scores helps one to assess the goodness of the various winding configurations. Hence, the configuration that has triple-layer winding performs the best among others and the double-layer version 3 configuration comes next. Although the secondary score of the single-layer winding yields a higher score, the primary score of the double-layer version 3 winding is better than the single-layer one. This result can also be reached by observing the Pareto frontier solutions sets given in Fig. 8a, the best-performed configuration is placed close to the right bottom corner. The Pareto front solutions of the other configurations move to the upper left corner as the performance is degraded. However, it is hard to distinguish the quality of the multiple Pareto front solutions when they get close to each other. Thanks to the score-based comparison, a clear assessment can be made.

6 Conclusions

This article investigated a 2-pole Line Start Synchronous Reluctance Machine (LS-SynRM) with multiple multilayer (ML) winding configurations to assess the tradeoff between winding MMF harmonics and end winding length. In all considered ML winding configurations, the number of turns in each coil group is unevenly distributed to a 24-slot stator. Initially, the percentages of each coil number of turns in a coil group were optimized using a multi-objective algorithm for all winding types. After this process, six Pareto front sets were generated for the six winding configurations. From these sets, three distinct results were selected: the one with the minimum THD, the one with the minimum EWS and less than 20% THD, and the one in between. A total of sixteen candidate winding configurations were selected for the second stage of optimization. One configuration was the conventional single-layer configuration, and the remaining fifteen comprised three different turn number ratios from each of the five multilayer winding configurations. The optimization process is carried out with the aim of minimizing motor mass and loss, while also taking into account the constraints of torque ripple and phase voltage. After collecting all the Pareto optimal solutions, a newly proposed score-based Pareto front quality assessment method was employed to quantify and select the best winding configuration. Based on the results, it was concluded that winding configurations with lower harmonic content yield higher torque density and lower torque ripple. Accordingly, the triple-layer winding demonstrated the best performance, followed by the third version of the double-layer winding in comparison to other windings. Since the manufacturing complexity and the cost are also important parameters to be considered, double-layer winding stands forward as a good alternative to the triple-layer winding. Also, compared to the conventional single-layer winding, a significant efficiency improvement and torque ripple reduction are also achieved with the low harmonic content multilayer windings.

Acknowledgements We thank The Scientific and Technological Research Council of Turkey (TUBITAK) for supporting our research (Grant number 121E413).

Authors' Contributions DT and BT wrote the main manuscript text, prepared the figures and tables. MMC, BT and DT wrote the optimization algorithm in MATLAB environment and prepared the finite element analysis of the motor model in Ansys Maxwell. All authors reviewed the manuscript.

Funding This work was funded by The Scientific and Technological Research Council of Turkey (TUBITAK) under Grant number 121E413.

Data Availability The datasets generated during and/or analyzed during the current study are available from the corresponding author on reasonable request.

Declarations

Conflict interest The authors have no competing interests to declare that are relevant to the content of this article.

References

Abdel-Khalik AS, Ahmed S, Massoud AM (2015) Low space harmonics cancelation in double-layer fractional slot winding using dual multiphase winding. IEEE Trans Magn. https://doi.org/10.1109/TMAG.2014.2364988

Barcaro M, Bianchi N (2010) Air-gap flux density distortion and iron losses in anisotropic synchronous motors. IEEE Trans Magn 46:121–126. https://doi.org/10.1109/TMAG.2009.2030675

Bekka N, Zaim MEH, Bernard N, Trichet D (2016) A novel methodology for optimal design of fractional slot with concentrated windings. IEEE Trans Energy Convers 31:1153–1160. https://doi.org/10.1109/TEC.2016.2552546

Bianchi N, Bolognani S, Bon D, Pré MD (2009) Rotor flux-barrier design for torque ripple reduction in synchronous reluctance and PM-assisted synchronous reluctance motors. IEEE Trans Ind Appl 45:921–928. https://doi.org/10.1109/TIA.2009.2018960

Cistelecan MV, Ferreira FJTE, Popescu M (2010) Three phase tooth-concentrated multiple-layer fractional windings with low space harmonic content. In: 2010 IEEE energy conversion congress and exposition, ECCE 2010—Proceedings 1399–1405. https://doi.org/10.1109/ECCE.2010.5618267

Cupertino F, Pellegrino G, Gerada C (2014) Design of synchronous reluctance motors with multiobjective optimization algorithms. IEEE Trans Ind Appl 50:3617–3627. https://doi.org/10.1109/TIA.2014.2312540

Dajaku G, Xie W, Gerling D (2014) Reduction of low space harmonics for the fractional slot concentrated windings using a novel stator design. IEEE Trans Magn. https://doi.org/10.1109/TMAG.2013.2294754

Dajaku G, Spas S, Gerling D (2019) Advanced optimization methods for fractional slot concentrated windings. Electr Eng 101:103–120. https://doi.org/10.1007/s00202-019-00760-6

Dajaku G, Gerling D (2012) Different novel methods for reduction of low space harmonics for the fractional slot concentrated windings. In: ICEMS 2012—Proceedings: 15th international conference on electrical machines and systems

De AAT, Member S, Ferreira FJTE, Member S (2014) Beyond induction motors—technology trends to move up efficiency. IEEE Trans Indus Appl 50:2103–2114. https://doi.org/10.1109/TIA.2013.2288425

EL-Refaie AM (2010) Fractional-slot concentrated-windings synchronous permanent magnet machines: opportunities and challenges. IEEE Trans Industr Electron 57:107–121. https://doi.org/10.1109/TIE.2009.2030211

Gamba M, Pellegrino G, Vagati A (2015) A new PM-assisted synchronous reluctance machine with a nonconventional fractional slot per pole combination. J Electr Eng 15:97–104

Gundogdu T, Komurgoz G (2019) Investigation of winding MMF harmonic reduction methods in IPM machines equipped with FSCWs. Int Trans Electr Energy Syst 29:1–27. https://doi.org/10.1002/etep.2688

Kabir MA, Husain I (2016) New multilayer winding configuration for distributed MMF in AC machines with shorter end-turn length. In: IEEE power and energy society general meeting 2016-Novem, pp 0–4. https://doi.org/10.1109/PESGM.2016.7741756

Kabir MA, Husain I (2018) Application of a multilayer AC winding to design synchronous reluctance motors. IEEE Trans Ind Appl 54:5941–5953. https://doi.org/10.1109/TIA.2018.2859033

Kim H, Park Y, Oh ST et al (2020) A study on the rotor design of line start synchronous reluctance motor for ie4 efficiency and improving power factor. Energies (basel). https://doi.org/10.3390/en13215774

Kocabas DA (2009) Novel winding and core design for maximum reduction of harmonic magnetomotive force in AC motors. IEEE Trans Magn 45:735–746. https://doi.org/10.1109/TMAG.2008.2005532

Kurihara K, Wakui G, Kubota T (1994) Steady-state performance analysis of permanent I. IEEE Trans Magn 30:1306–1315

Lipo TA (1991) Synchronous reluctance machines-a viable alternative for ac drives? Electric Mach Power Syst 19:659–671. https://doi.org/10.1080/07313569108909556

Lipo TA (2017) Introduction to AC machine design. Wiley, Hoboken

Mingardi D, Bianchi N (2017) Line-start PM-assisted synchronous motor design, optimization, and tests. IEEE Trans Indus Electron. https://doi.org/10.1109/TIE.2017.2711557

Pyrhönen J, Jokinen T, Hrabovcová V (2008) Design of rotating electrical machines

Sato S, Sato T, Igarashi H (2015) Topology optimization of synchronous reluctance motor using normalized gaussian network. IEEE Trans Magn. https://doi.org/10.1109/TMAG.2014.2359679

Spargo CM, Mecrow BC, Widmer JD (2013) Application of fractional slot concentrated windings to synchronous reluctance machines. In: Proceedings of the 2013 IEEE international electric machines and drives conference, IEMDC 2013, pp 618–625. https://doi.org/10.1109/IEMDC.2013.6556159

Stojceska V, Parker N, Tassou SA (2022) Reducing GHG emissions and improving cost effectiveness via energy efficiency enhancements: a case study in a biscuit industry. Sustainability (switzerland). https://doi.org/10.3390/su14010069

Tekgun D, Alan I (2022) A new oval shaft, high performance, 2 pole line start synchronous reluctance machine for submersible pump applications. Int J Appl Electromagnet Mech 70:73–93. https://doi.org/10.3233/JAE-220026

Tekgun D, Muhsin Cosdu M, Tekgun B, Alan I (2021) Investigation of the effects of multi-layer winding structures in two pole synchronous reluctance machines. Proceedings - 2021 IEEE 3rd Global Power Energy and Communication Conference, GPECOM 2021:120–125. https://doi.org/10.1109/GPECOM52585.2021.9587567

Tessarolo A, Mezzarobba M, Barbini N (2016) Improved four-layer winding design for a 12-slot 10-pole permanent magnet machine using unequal tooth coils. IECON proceedings (industrial electronics conference), pp 1686–1691. https://doi.org/10.1109/IECON.2016.7793399

Vagati A, Pastorelli M, Franceschini G, Petrache SC (1998) Design of low-torque-ripple synchronous reluctance motors. IEEE Trans Ind Appl 34:758–765. https://doi.org/10.1109/28.703969